Supplementary information for "Phospholipase-catalyzed degradation drives domain morphology and rheology transitions in model lung surfactant monolayers"

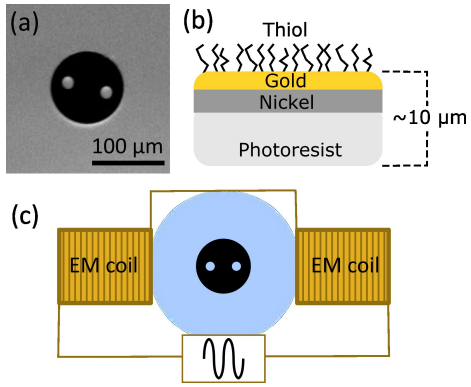

Fig. S1 (a) Top view brightfield image of ferromagnetic microbutton probe. (b) Schematic diagram of the fabricated layers of the microbutton probe. The nickel layer provides the ferromagnetic properties of the microbutton and the thiol layer enables the amphiphilicity of the probe as described elsewhere.[23] (c) Schematic diagram of the microbutton probe placed on an air-water interface in the center of two electromagnets connected in series, used to apply an external torque on the probe.

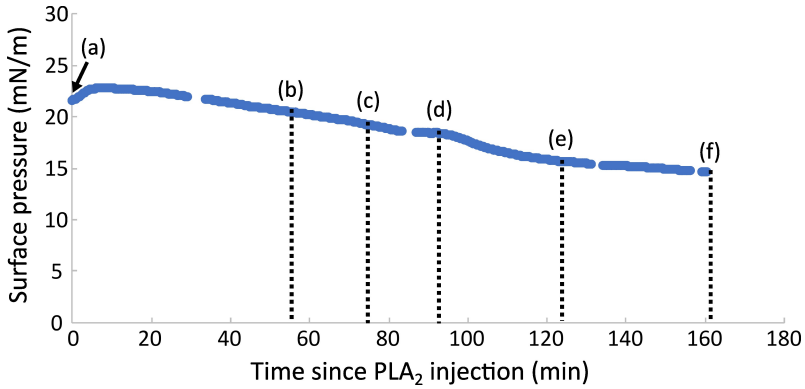

Fig. S2 Surface pressure versus time since PLA_2 injection plot of the degrading monolayer displayed in Fig. 4 (main text). Labels a-f correspond to the images labeled in Fig. 4 (main text). Once PLA_2 is injected, surface pressure initially rises, which is posited to be from PLA_2 adsorption to the interface. The rise in surface pressure is followed by decay throughout the remainder of the experiment. The minor feature in the surface pressure around (d) is unique to this experiment and was not seen with other monolayers. Surface pressure decreases steadily with time, and shows no qualitative features that would correlate with monolayer transitions or changes in morphology.

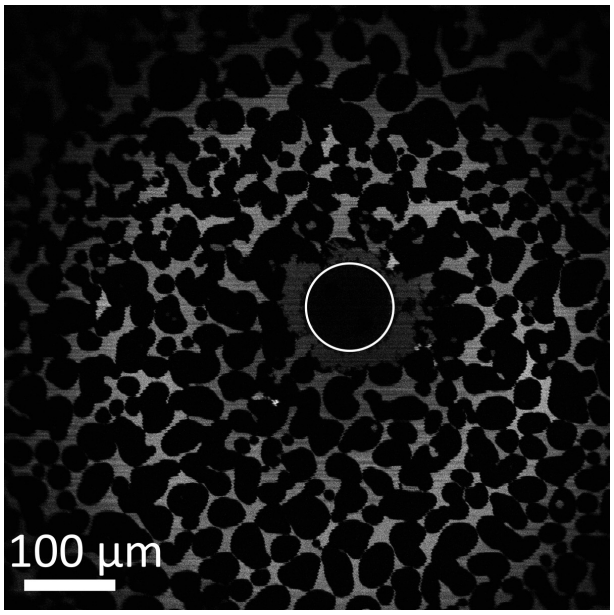

Fig. S3 Larger field of view fluorescence micrograph of Fig. 4d (main text), showing domains that are aggregated (but not coalescing), akin to a 2D colloidal gel whose network spans the interface. Note that in this experiment, degradation detached the disk from the network. In such cases, rheology is not reported after detachment; only morphology is tracked.

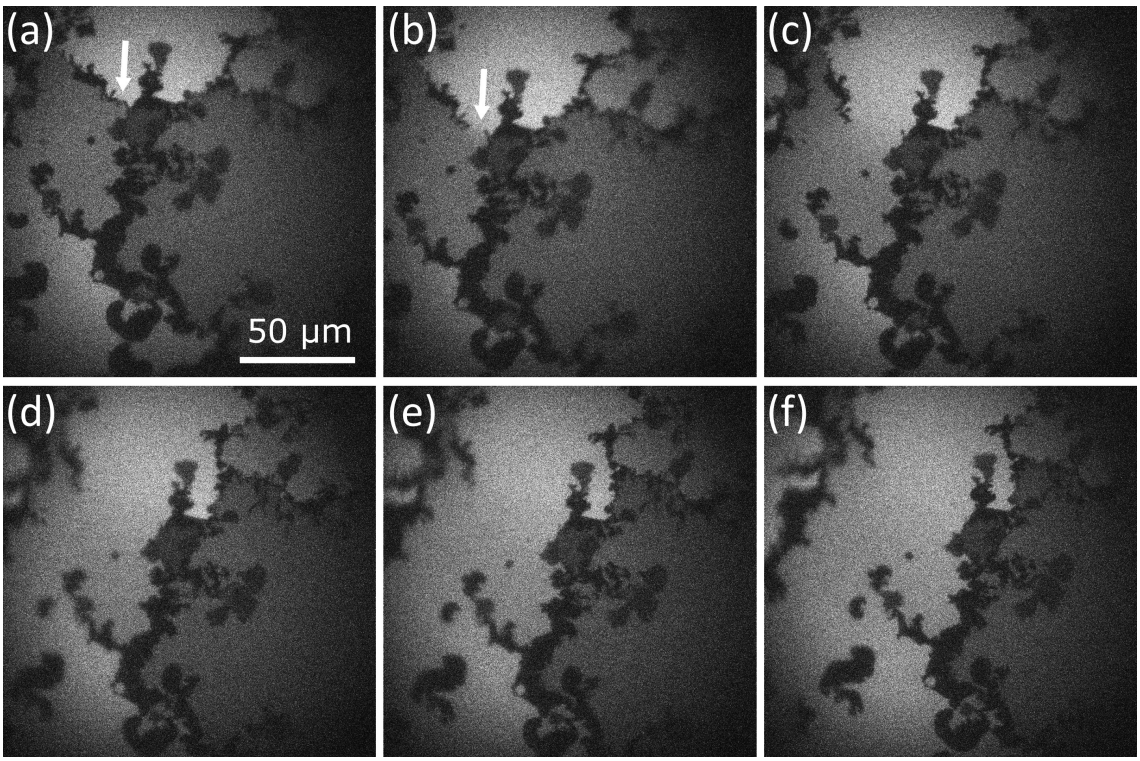

Fig. S4 Fluorescence micrographs tracking network breakage event and corresponding mixing of formerly distinct pockets of disordered phase. (a) White arrow indicates network bridge prior to breakage. Disordered phase above and below have differing fluorescence intensities, indicating distinct pockets separated by the network. (b) White arrow points at breakage location. Front of higher fluorescence intensity is visibly passing through the breakage area, showing the initial diffusive mixing of the two disordered regions. (c-e) Fluorescence intensities continue to equilibrate, reaching a fully mixed, uniform intensity in (f).

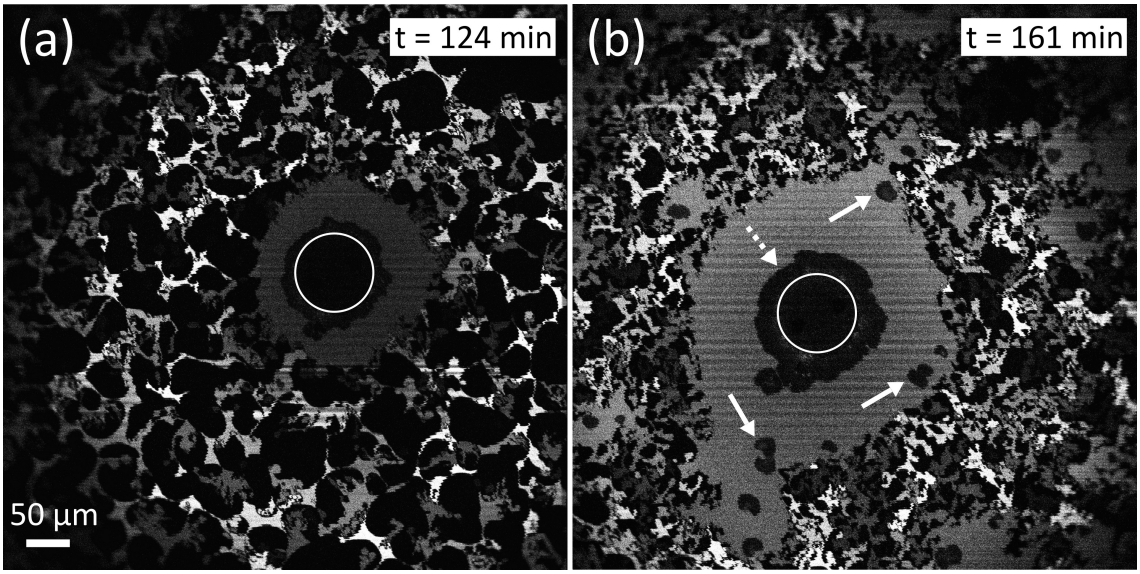

Fig. S5 Larger field of view fluorescence micrographs of (a) Fig. 4e and (b) Fig. 4f from the main text. Micrographs show on a larger scale the impact of network erosion. Like in Figure S3, rheology data is not reported after probe detachment. Condensed domains lining each probe (dashed arrow) are understood to be a mixture of DPPC and PA bound with PLA_2 in the subphase, the same as the domains which nucleate at late stages of degradation (solid arrows), as discussed in Figure 6 of the main text.

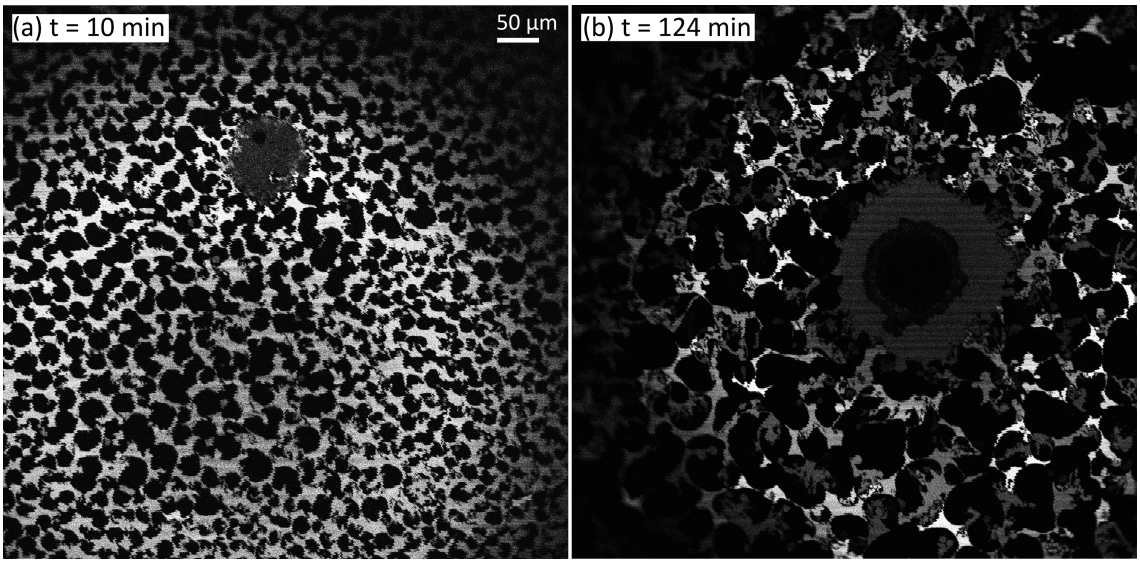

Fig. S6 Larger field of view fluorescence micrographs of (a) Fig. 7c and (b) Fig. 7c inset from the main text. Initial solid-like networks when using relatively fresh (a) or aged (b) PLA_2 show distinct morphologies. For the monolayer in (b), the probe was connected until t $\backsim$ 100 minutes; rheology data prior to probe detaching is reported in Fig. 9 in the main text.

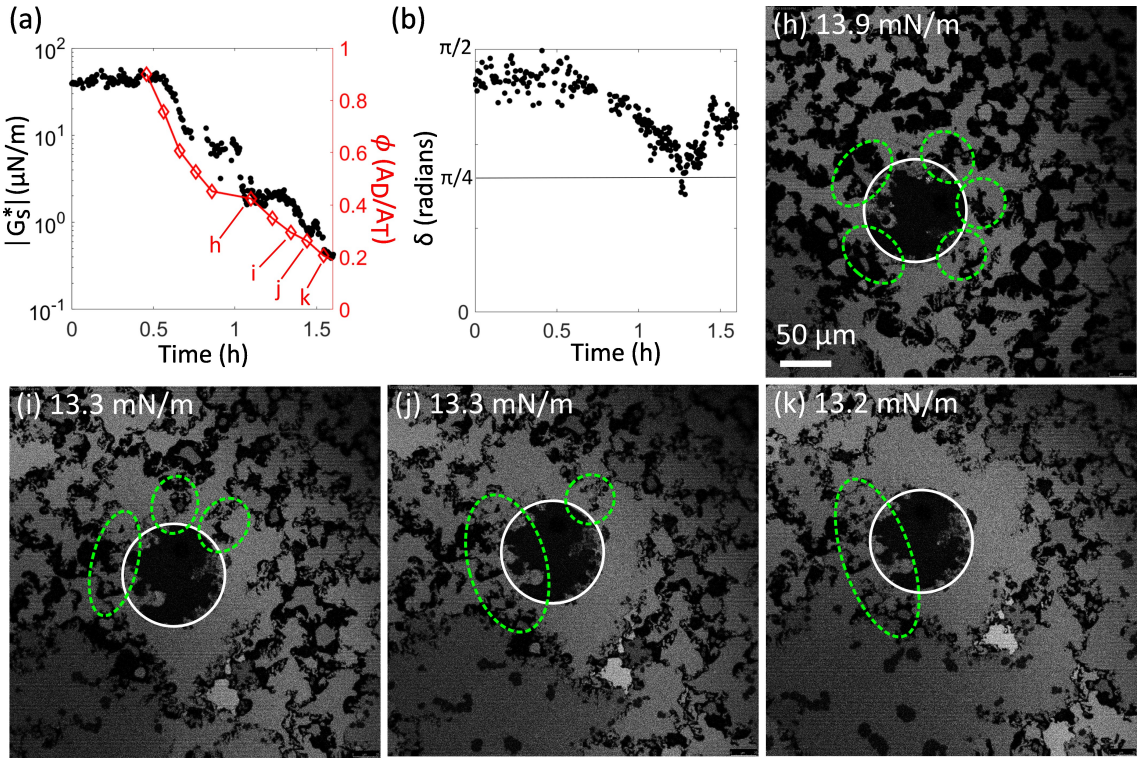

Fig. S7 (a) and (b) reproduce Fig. 8 in the main text. The fluorescence micrographs (h-k) correspond to the (h-k) labels in the interfacial rheology data. Micrographs show the points of contact between the condensed phase network and the microbutton probe, outlined in green dashes, transitioning from five points initially distributed around the probe (h), to three points (i), two points (j), and finally one (k).